ACS APPLIED MATERIALS & INTERFACES

RESEARCH ARTICLE

www.acsami.org

Field Emission Properties of Low-Temperature, Hydrothermally Grown Tungsten Oxide

Maria Trapatseli,[†] Dimitra Vernardou,[†,‡,§] Panagiotis Tzanetakis,[⊥,∥] and Emmanuel Spanakis[†,⊥,*]

[†]Department of Materials Science and Technology and [∥]Physics Department, University of Crete, 710 03 Heraklion, Crete, Greece

[‡]Center of Materials Technology and Photonics and [§]Science Department, School of Applied Technology, Technological Educational Institute of Crete, 710 04 Heraklion, Crete, Greece

[⊥]Institute of Electronic Structure and Laser, Foundation for Research & Technology—Hellas, Vassilika Vouton, 711 10 Heraklion, Crete, Greece

ABSTRACT: Tungsten oxide layers have been prepared on conductive glass substrates using aqueous chemical growth from a sodium tungstate precursor at low-temperature hydrothermal conditions. The deposits were then tested as cold electron emitters. Traceable layers could be deposited only within a narrow pH range of 1.5−2 at a time length not exceeding 4 h. Transmittance in the visible spectrum was found to decrease with deposition time. The presence of both monoclinic and hexagonal phases was always detected. At the longest deposition times and highest precursor concentrations, morphologies comprise randomly oriented spikes or rods. The overall emission performance is found to improve with growth time and precursor concentration. The role of morphology on the emission properties of the films is discussed.

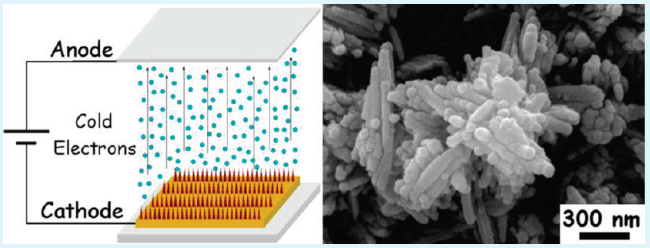

KEYWORDS: sodium tungstate, Raman, cold cathode, rods, WO_3, Fowler−Nordheim

INTRODUCTION

Tungsten trioxide, WO_3, has long been well-known and pursued as an electrochromic material. Its optical transmittance can be altered from a "colored" to a "bleached" state and vice versa by application of specific bias voltages. Electrochromism is required for smart window and certain backlit display applications.[1] Tungsten trioxide has also been proposed as a gas sensor, and a notable amount of research effort has been devoted to its photocatalytic property for either dissociation of organic pollutants[2] or clean energy production through water splitting.[3] Being a moderately wide band gap material (2.5−3.5, depending on the lattice structure),[4] it has the quality of a satisfactory optical transparency combined with poor but measurable electrical conductivity (10^{-2}−10^{-3} Ω^{-1} cm^{-1}) on the same order as that of intrinsic silicon. Conductivity is suggested to increase in the presence of oxygen vacancies.[5] The fact that conventional high-temperature preparation methods, such as thermal evaporation of tungsten, produce oxide films comprising sharp, high-aspect ratio structures such as rods or spikes has recently triggered the idea that WO_3 could be used as a cold electron-emitting source, likewise called a "field emitter".[6−9]

In vacuum electronics, a field emitter is actually the surface of an at least semiconducting material that permits, under sufficient cathodic bias, the extraction of electrons by quantum mechanical tunneling through a triangle-shaped potential barrier. The zero-bias height of the barrier is the work function of the surface. The required electric field for emission is very high, on the order of 10^8 V/cm,[10] and thus difficult to achieve between planar electrodes. On the other hand, structuring the emitter surface with sharp, potentially perpendicularly oriented, one-dimensional structures enhances the field at their apexes with respect to the mean applied field facilitating emission.[11] Several different families of materials, such as metals, nitrides, silicon,[12] and carbon based compounds,[13] etc., and different surface structures, such as rods, tubes, spikes, etc., have been tested as field emitters over the years, sometimes with great success.[14] Among these are metal oxides, mostly those of zinc, molybdenum, and tungsten.[4,14] Potential applications of field emitters include electron guns, rf power sources, and amplifiers as well as flat panel displays and lamps.[15,16]

The research presented here addresses specific metal oxide cathode requirements in field emission applications, such as displays and flat lamps. These are transparency to visible light, low cost, and easy of fabrication of emitters over large-area substrates, including flexible ones. The specific goal was to find a way to grow adherent and sharp WO_3 structures at reasonable processing times, employing temperatures low enough to be sustained by most flexible, usually organic, substrate materials. We have selected a simple, "one-pot", hydrothermal synthesis route because it is an inherently low-temperature, low-cost technique that can be scaled up and in which the morphological characteristics of deposited metal oxides can be tuned by a careful choice of reaction parameters such as solution chemistry, temperature, and time.[2] By this, we have been able to deposit WO_3 on top of transparent conducting substrates with adequate adherence at 110 °C using

Received: April 28, 2011
Accepted: June 20, 2011
Published: June 20, 2011

Table 1. Sample Preparation Parameters

sample no.	sample i.d.	Na_2WO_4 concn (M)	pH modifier	NaCl concn (M)	reaction time (h)
1	w57a	0.125	HNO_3	0	1
2	w45a	0.125	HNO_3	0	2
3	w46a	0.125	HNO_3	0	3
4	w47a	0.125	HNO_3	0	4
5	w64a	0.060	HNO_3	0	4
6	w65a	0.030	HNO_3	0	4
7	w66a	0.015	HNO_3	0	4
8	w63a	0.125	HCl	0	4
9	w51a	0.125	HCl	0.060	4
10	w52a	0.125	HCl	0.125	4
11	w53a	0.125	HCl	0.250	4

sodium tungstate (Na_2WO_4) as the precursor. We examine the role of growth time and of the presence of additives (such as NaCl,[17]) in the solution on the optical properties, chemical character, and morphology of the films. We report for the first time that these WO_3 structures indeed have the potential to emit electrons at reasonable electric fields and comment on the dependence of this emission on the deposition conditions, with comparison to other state-of-the-art metal oxide cold cathodes.

EXPERIMENTAL SECTION

Tungsten oxide thin films were deposited on indium tin oxide (ITO)-coated glass substrates. The coating had a nominal surface resistance of 15 Ω/sq. Aqueous chemical growth was conducted with 10 mL deionized water solutions in 22 mL glass vials in which the substrate was always placed horizontally at the bottom of the vial. We have chosen a temperature of 110 C for the hydrothermal reaction because it is low but higher than the normal boiling point of water, ensuring enhanced dilution capability through intensified molecular motion, and is also the highest attainable by common vial caps. The precursor, used at different molarities, was analytical grade sodium tungstate, Na_2WO_4, diluted in an acidic environment.[17,18] The acid is necessary for the intermediate synthesis of H_2WO_4 from which WO_3 is produced during hydrolysis.[17] In our case, the pH value was adjusted to 1.65 ± 0.05 by adding dropwise 10 M concentrated nitric into the solution under continuous stirring.[19] We have observed that the reaction is very sensitive to the pH value. Below 1.5, gelation and subsequent precipitation occurs uncontrollably, even at room temperature, whereas above 2.0, it takes much longer than 5 h for any deposition to occur.

Finally, we have tried the incorporation of NaCl in the solution because it has been shown that certain salts can promote synthesis of sharper structures, at least for higher temperatures and reaction times.[17,19] In this case, hydrochloric acid was used as the pH modifier instead of HNO_3 in an effort not to increase the number of reacting species in the solution. After each predetermined reaction, time samples were rinsed with deionized water and dried at 70 °C for 30 min in atmospheric conditions. We have verified from thermogravimetric analysis that hydrates are removed from the films at 250 °C;[1,20] thus, all samples were calcined at that temperature for 90 min.

Optical characterization of the films was performed by taking transmittance spectra in the range between 250 and 1100 nm using a Perkin-Elmer Lambda 950 UV−vis−NIR spectrophotometer with an integrating sphere. Qualitative Raman chemical analysis was performed using the 473 nm laser beam of a Nicolet Almega XR micro-Raman system with 100 μm pinhole, allowing for a maximum spectral resolution of 19 cm^{-1}. Each spectrum is the average of at least five consecutive sample and background scans. Scanning electron microscopy (SEM) was carried out using a Jeol JSM-7000F field-emission microscope after sputter-coating each sample with a 20-nm-thick film of gold. Field emission current versus voltage ($I-U$) curves were acquired under high-vacuum conditions of 10^{-3} Pa or lower in a planar diode system described in detail elsewhere.[21] The substrate-to-anode distance was kept to 100 μm. Several conditioning runs were always conducted before the final stable and reproducible curves were recorded.[10,22] Each $I-U$ curve is the average of at least three current−voltage scans, and each current value in a scan is the average of 10 measurements at that voltage.

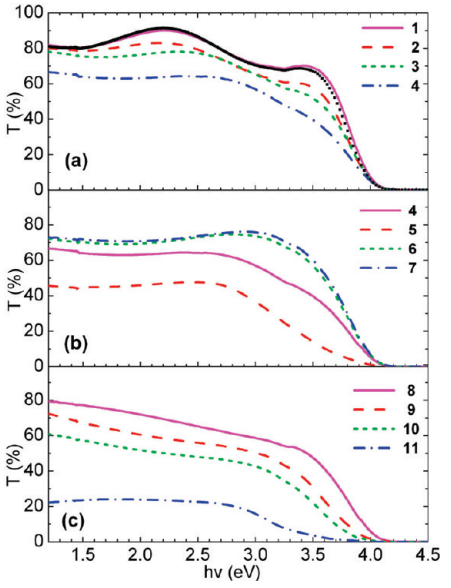

Figure 1. Transmittance, T, vs photon energy, hv, for all samples of this study (see Table 1). (a) Samples 1−4, increasing deposition time (1−4 h); (b) samples 4−7, decreasing Na_2WO_4 concentration (0.125−0.015 M); and (c) samples 8−11, increasing NaCl concentration (0.060−0.25 M). Solid symbols are for the bare, ITO-coated substrate.

RESULTS

Table 1 lists preparation conditions for all samples employed in this study. Samples 1−4 were prepared at different reaction times; samples 4−7, with different HNO_3 concentrations; and samples 8−11, under the presence of NaCl at different concentrations. All samples had a white to yellowish color and were conductive along the surface, indicating that the conductive layer is unaffected by the reacting agents. Figure 1 presents the

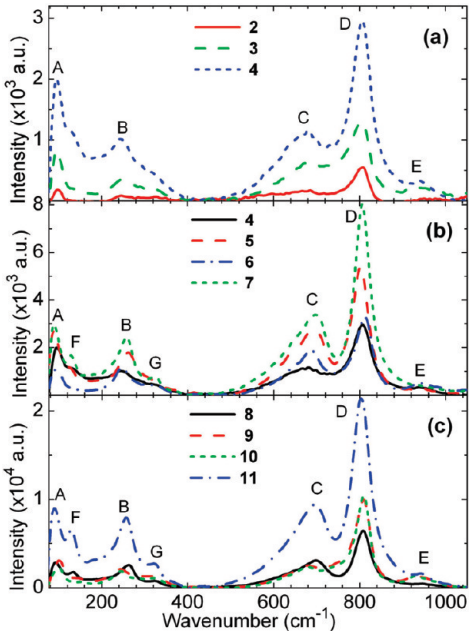

Figure 2. Raman spectra for the samples of this study. (a) Samples 2−4, increasing deposition time (2−4 h); (b) samples 4−7, decreasing Na_2WO_4 concentration (0.125−0.015 M); and (c) samples 8−11, increasing NaCl concentration (0.060−0.25 M).

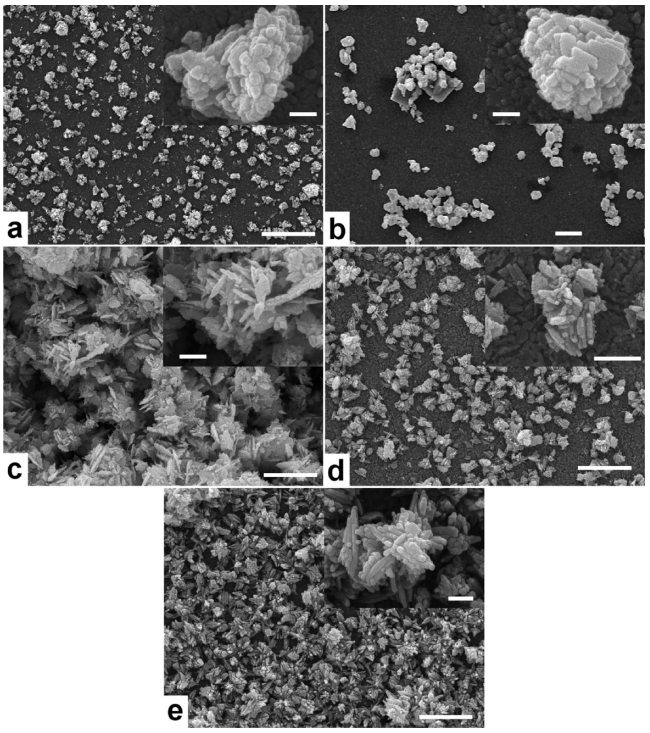

Figure 3. Scanning electron micrographs of selected samples with magnification insets. (a) Sample no. 2, deposited at the second longest time of 2 h. Scale bar, 2 μm; inset, 200 nm. (b) Sample no. 7 deposited with the lowest Na_2WO_4 concentration. Scale bar, 5 μm; inset, 200 nm. (c) Sample no. 4, deposited at the highest time. Scale bar, 2 μm; inset, 500 nm. (d) Sample no. 8, same as no. 4, but with HCl instead of HNO_3. Scale bar, 2 μm; inset, 500 nm. (e) Sample no. 10, deposited at the 1:1 Na_2WO_4/NaCl ratio. Scale bar, 2 μm; inset, 200 nm.

transmittance curves of the samples along with the reference transmittance of the ITO-coated glass substrate. In the low absorption region, the transmittance spectrum of ITO is affected by interference fringes. It is obvious that the transmittance of the WO_3 layers decreases with increasing deposition time as a result of an increase in the deposited mass. On the other hand, the transmittance of WO_3 generally increases at lower Na_2WO_4 precursor concentration. When NaCl is added into the solution, a monotonic reduction of transmittance is observed with increasing NaCl concentration. In most of the samples, the visible range transmittance remains above 50%, allowing for applications for which partial transparency is desired.

Figure 2 presents results of the micro-Raman characterization of the films. The intensity of the peaks is generally inversely correlated to their visible transmittance, that is, proportional to the deposited mass. As a consequence, no signal could be detected from sample 1, which agrees with its transmittance being similar to that of the uncoated substrate. Five peaks, marked as A, B, C, D, E in the graphs of Figure 2, could always be detected. These correspond to wavenumbers 94, 250, 687, 807, and 940 cm^{-1}, respectively. The F = 130 cm^{-1} and G = 323 cm^{-1} could be identified only for samples 7, 8, and 11, which showed the highest scattering intensity in the series. All peaks match known characteristic lines of WO_3 within the resolution of our instrument.[23,24] The E line is associated with the stretching vibration of W═O terminal bond, and its low intensity indicates the absence of any significant fraction of hydrates in the layers after thermal treatment. C and D lines correspond to the stretching vibrations of the W−O bonds; B and G lines, to the bending (deformation) vibrations of the O−W−O bonds. Finally, the A and F lines are assigned to lattice modes.[23,24]

Comparative SEM images of the surface morphology for five epresentative cases, samples 2, 4, 7, 8 and 10, are shown in Figure 3. As a general observation, one can say that WO_3 is deposited in the form of particulates that may vary in density, size, and texture, depending on the deposition conditions. From Figure 3a,c, we find that the density and size of particulates increases with deposition time. From Figure 3b,c, we also observe that reduction of Na_2WO_4 has a pronounced effect on particulate density and size. WO_3 grown using 0.015 M Na_2WO_4 (no. 7) shows a smaller density of generally larger, coalesced, particles than the material grown with 0.125 M precursor concentration (no. 4). At the highest concentration and deposition time (0.125 M, 4 h), the particulates contain certain spike-like features having a random orientation and an approximate length of 400 nm (Figure 3c). The change of the pH modifier, from HNO_3 in no. 4 to HCl in no. 8, with all other conditions identical, reduces the size and density of the particulates. Each particulate now consists of mainly coalesced rods, which are smaller and blunter compared with those found with HNO_3 (no. 4). Figure 3e shows that the addition of NaCl does not affect the size of particulates but increases their density, and each particulate seems to consist of a larger volume percentage of rods compared with the NaCl-free case [Figure 3d).

Field emission data of all samples, categorized with respect to deposition conditions, are shown in Figure 4. The current density, J, is calculated from the measured current divided by the anode electrode surface, and the field, F, is the ratio of bias voltage to the interelectrode distance. No current could be extracted from the bare ITO coating within the F range of our experiments. All curves of Figure 4 show the known three regions

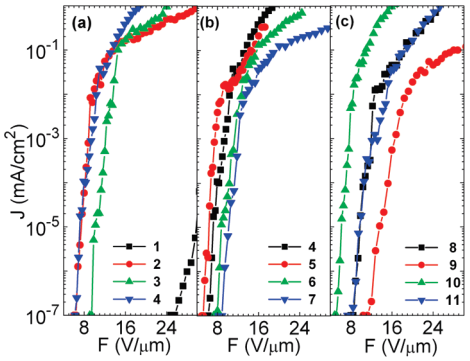

Figure 4. Electron emission current density, J as a function of applied mean field, F. (a) Samples 1−4, increasing deposition time (1−4 h); (b) samples 4−7, decreasing Na_2WO_4 concentration (0.125−0.015 M); and (c) samples 8−11, increasing NaCl concentration (0.060−0.25 M).

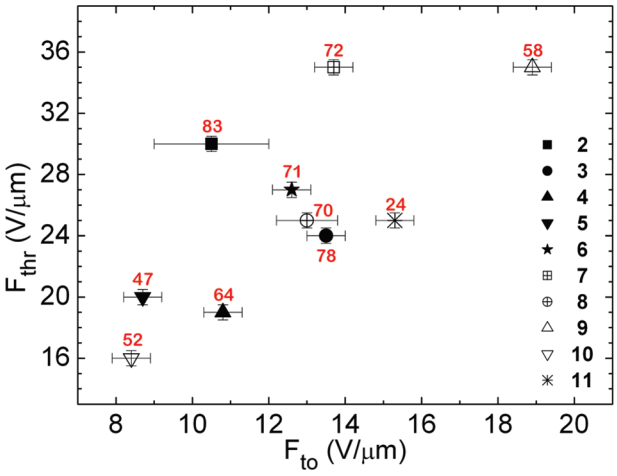

Figure 5. Threshold, F_{thr}, as a function of turn on, F_{to} electron emission field for all samples of this study. Sample numbers are shown in the legend. The label beside each symbol gives the transmittance of the corresponding sample at 2.2 eV photon energy. Data are compiled from Figures 1 and 4. Error bars give a measure of uncertainty in the field values coming from the statistical variation of current measurements.

of a typical field-emission spectrum:[25] (a) the zero-emission region, below a certain onset voltage, where no signal can be detected; (b) the field-emission region in which a steep rise of current with bias is observed; and (c) the saturation region, at high bias, where a significant reduction of the slope is observed. If we define the turn-on field, F_{to}, as the one that extracts 10 μA/cm^2 current density and the threshold field, F_{thr}, as the one that results in the highest measured density of 1 mA/cm^2, then we find that overall performance (low F_{to} and F_{thr}) is improved with deposition time. Reduction of the Na_2WO_4 concentration generally deteriorates emission. Finally, addition of NaCl seems to improve emission at the ratio of Na_2WO/NaCl =1 (sample 10) compared with the salt-free case (sample 8). Critical field values are depicted in the graph of Figure 5. F_{to}, as defined above, is commonly used in the literature as a figure of merit for emission performance.[4,14]

DISCUSSION

As already demonstrated in the literature, WO_3 can be grown by the hydrothermal method from a sodium tungstate precursor.[17,18,20,26,27] All efforts resulted in the production of powders. Temperatures around 160 °C and hydrothermal reaction times of 12 h or higher were utilized. We have shown that the material can be formed as a deposit at temperatures as low as 110 °C and reaction times of 4 h at max, with adhesion that is good enough on ITO-coated substrates for field emission and potentially other coating-related applications. For this, it is crucial to have a delicate balance between pH and reaction temperature. At lower pH, gelation and subsequent precipitation occurs rapidly, even at lower temperatures, but the deposit adheres poorly to the substrate and cannot be rinsed without loss. For higher pH, higher temperature or longer reaction time is necessary for deposition.

Pure WO_3 is obtained in all deposits, as judged from the fact that we were able to associate all Raman peaks with known material vibrations, even in the case that NaCl was added to the original solution. This is not a priori expected for such a low temperature wet chemical technique. Known WO_3 hydrates are not observed in our study. $WO_3 \cdot H_2O$ and $WO_3 \cdot 2H_2O$ have distinctively different peak positions,[23] and $WO_3 \cdot 1/2H_2O$ shows a relative intensity between the main C (687 cm^{-1}) and D (807 cm^{-1}) peaks that is opposite to what is observed here. The D peak (807 cm^{-1}) is the strongest in all cases, and its position matches that known for monoclinc WO_3. A and F line wavenumbers concur with that phase within the resolution of our experiments. On the other hand, B (250 cm^{-1}) and C peaks are characteristic of the hexagonal structure, and G can equally be attributed to both. We therefore suggest that a mixed phase of monoclinic and hexagonal WO_3 is produced. This agrees with the fact that the monoclinic is known to be the stable phase from room temperature up to 330 °C[28,29] but also with the observation that the metastable hexagonal structure is often traced in chemical fabrication routes involving hydrogen or alkaline atoms,[29] especially at pH values in the range of 1.5−2.0.[18]

WO_3 is known to have a natural tendency to grow in 1D or 2D structures, such as platelets and rods or wires, both under high-T thermal evaporation treatments of tungsten metal or oxide precursors[6−9] and under hydrothermal environments at relatively high temperatures and long reaction times.[19,26] In the latter case, the presence of salts, such as NaCl, Na_2SO_4 or K_2SO_4, etc., inside the solution promotes unidirectional growth through the capping action of salt anions along the crystallographic axes perpendicular to the growing direction.[17,19,20,30−32] This study has demonstrated that preferentially oriented structures can be produced even after only 4 h of reaction at a temperature as low as 110 °C. For this, the precursor concentration must not drop below a critical value, since this has a negative impact on the sharpness of the structures (Figure 3b). The presence of NaCl does not cease to promote the unidirectional WO_3 growth over the total material volume through the salt's aforementioned capping action. On the other hand, the length or orientation of these structures does not improve in our experiments with the use of this salt.

The field emission (FE) performance of a candidate cathode is expected to depend on certain factors, such as (a) the presence of sharp 1D or 2D structures, oriented normal to the surface and dispersed at a low density over the surface, (b) low work function of the emitters at operation conditions, and (c) good electrical conductivity of the cathode material. This study gives a first result on the field emission capability of wet chemically grown WO_3, although only 1D structuring has been sought and preliminarily

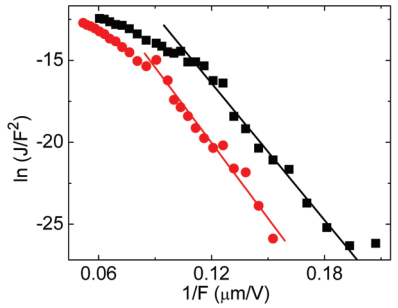

Figure 6. Fowler−Nordheim plots of data of Figure 4 for selected samples nos. 4 (circles) and 10 (squares) (see text).

achieved. It is, indeed, found that best performance of samples such as no. 4 ($F_{to} \sim 11$ V/μm, $F_{thr} \sim 19$ V/μm) prepared at the longest reaction time and no. 10 ($F_{to} = 8$ V/μm, $F_{thr} = 16$ V/μm) prepared with a 1:1 ratio of Na_2WO_4/NaCl, coincides with the presence of elongated features on their surface. On the other hand, longer reaction times or higher NaCl concentrations promote thick film formation, which may deteriorate emission if either the geometry of the structures blunts or electron emission starts to get limited by the limited conductivity of WO_3. The latter may actually be the reason for the poor emission performance of sample no. 11, which has the thickest deposition, verified by its ultralow transmittance in the visible range (Figure 1).

To check whether the Fowler−Nordheim (FN) field-assisted electron tunneling mechanism is responsible for emission, we show in Figure 6 the FE data for the best samples, 4 and 10, in the so-called FN plot. Since FN current density, J, obeys $J = A\cdot(\beta F)^2\cdot\exp(-b/\beta F)$,[33] then FE data points should fall on a straight line in this plot . This is, indeed, observed. The slope of the line is equal to $-b/\beta$, where $b = 0.94\cdot B\cdot\Phi^{3/2}$, Φ is the work function of the emitting surface and β is the *field enhancement factor.*[33] β is defined as the ratio of the local field at the emitters to the mean field and is a measure of the sharpness and directionality of the emitters. Assuming $\Phi = 5.7$ eV[4,7] for WO_3, we find from the slopes of Figure 6 a β of ∼600 for both cases. Although this is a good value, we can conclude that the geometry cannot yet compete with that of high-temperature thermally evaporated WO_3, in which 2−5 times lower turn-on voltages and 2−4 times higher field enhancement factors have already been accomplished[4,7,9] through fabrication of ultrahigh-aspect-ratio-oriented microstructures.

Finally, to assess the combined transparency and emission performance of our samples, we have plotted in Figure 5 the threshold vs the turn-on field for emission for each sample, including the transmittance at 2.2 eV (i.e., at the maximum of the bare conducting substrate) as a label at each data point. Sample 1 has been omitted because of its extremely high F_{to}. Best materials in terms of emission, discussed previously, are located at the lowest and left-most quadrant of this graph. They are, however, among the less transparent, having a transmittance of ∼55%. Samples 3, 6, and 8 seem to achieve the best compromise between transparency (over 70%) and emission performance. We suggest that this arises from a lower surface density of adequately sharp WO_3 microstructures (compare, for example, Figure 3d of sample 8 with 3e of sample 4 and 3c of sample 10). High surface density is known to induce screening effects on the field of each emitter due to the presence of its neighbors at close proximity, resulting in poor geometrical field enhancement.[34] Thus, if transparent WO_3 cold cathodes are to be considered, then the density of the structures must be reduced without deterioration of their beneficial geometry.

CONCLUSIONS

WO_3 microstructured layers were successfully grown on transparent conducting substrates by simple hydrolysis of Na_2WO_4 at the very low temperature of 110 °C and reaction time of 4 h with adequate adhesion for field emission applications. The role of pH proved crucial, permitting deposition only in a very limited range. The material consists of mixed monoclinic and hexagonal phases and is free of foreign compounds, even in the case that NaCl is included in the solution. Randomly oriented spikes or rods are observed in the high precursor concentration/long deposition time regime. NaCl increased the volume percent of rods in the material. The structures are partially transparent to visible light and capable of cold electron emission at moderate field strength through a Fowler−Nordheim tunneling process. Further work is needed toward improving the morphology of the deposits without altering the favorable temperature and duration conditions to match the field emission performance of their high-temperature thermal evaporation counterparts.

AUTHOR INFORMATION

Corresponding Author
*E-mail: spanakis@materials.uoc.gr.

ACKNOWLEDGMENT

The authors thank Mrs. Aleka Manousaki for her invaluable help with the SEM characterization

REFERENCES

(1) Granqvist, C. G. *Handbook of Inorganic Electrochromic Materials*; Elsevier: Amsterdam, 1995.
(2) Vernardou, D.; Drosos, H.; Spanakis, E.; Koudoumas, E.; Savvakis, C.; Katsarakis, N. *J. Mater. Chem.* **2011**, *21*, 513.
(3) Deb, S. K. *Sol. Energy Mater. Sol. Cells* **2008**, *92*, 245.
(4) Fang, X.-S.; Bando, Y.; Gautam, U. K.; Ye, C.; Golberg, D. *J. Mater. Chem.* **2008**, *18*, 509.
(5) Gillet, M.; Lemire, C.; Gillet, E.; Aguir, K. *Surf. Sci.* **2003**, *532−535*, 519.
(6) Zhou, J.; Ding, Y.; Deng, S. Z.; Gong, L.; Xu, N. S.; Wang, Z. L. *Adv. Mater.* **2005**, *17*, 2107.
(7) Huang, K.; Pan, Q.; Yang, F.; Ni, S.; He, D. *Appl. Surf. Sci.* **2007**, *253*, 8923.
(8) Li, Y.; Bando, Y.; Golberg, D. *Adv. Mater.* **2003**, *15*, 1294.
(9) Liu, J.; Zhang, Z.; Zhao, Y.; Su, X.; Liu, S.; Wang, E. *Small* **2005**, *1*, 310.
(10) Schwoebel, P. R.; Brodie, I. *J. Vac. Sci. Technol., B: Microelectron. Nanometer* **1995**, *13*, 1391.
(11) Utsumi, T. *IEEE Trans. Electron Devices* **1991**, *38*, 2276.
(12) Zorba, V.; Tzanetakis, P.; Fotakis, C.; Spanakis, E.; Stratakis, E.; Papazoglou, D. G.; Zergioti, I. *Appl. Phys. Lett.* **2006**, *88*, 081103.
(13) Karabutov, A. V.; Simakin, A. V.; Shafeev, G. A. *Surf. Interface Anal.* **2004**, *36*, 439.
(14) Xu, N. S.; Ejaz Huq, S. *Mater. Sci. Eng., R* **2005**, *48*, 47.
(15) Chen, J.; Dai, Y. Y.; Luo, J.; Li, Z. L.; Deng, S. Z.; She, J. C.; Xua, N. S. *Appl. Phys. Lett.* **2007**, *90*, 253105.
(16) Nakamoto, M. *IEEE Ind. Appl. Soc. Ann. Meet.* **2008**, 1.
(17) Wang, J.; Khoo, E.; Lee, P. S.; Ma, J. *J. Phys. Chem. C* **2008**, *112*, 14306.

(18) Whittingham, M. S.; Guo, J.-D.; Chen, R.; Chirayil, T.; Janauer, G.; Zavalij, P. *Solid State Ionics* **1995**, *75*, 257.
(19) Rajagopal, S.; Nataraj, D.; Mangalaraj, D.; Djaoued, Y.; Robichaud, J.; Khyzhun, O. Y. *Nanoscale Res. Lett.* **2009**, *4*, 1335.
(20) Yu, J.; Qi, L.; Cheng, B.; Zhao, X. *J. Hazard. Mater.* **2008**, *160*, 621.
(21) Spanakis, E.; Dialektos, J.; Stratakis, E.; Zorba, V.; Tzanetakis, P.; Fotakis, C. *Phys. Status Solidi, C* **2008**, *5*, 3309.
(22) Reuss, R. H.; Chalamala, B. R. *J. Vac. Sci. Technol., B: Microelectron. Nanometer* **2003**, *21*, 1187.
(23) Daniel, M. F.; Desbat, B.; Lassegues, J. C.; Gerand, B.; Figlarz, M. *J. Solid State Chem.* **1987**, *67*, 235.
(24) Delichere, P.; Falaras, P.; Froment, M.; Hugot-Le Goff, A.; Agius, B. *Thin Solid Films* **1988**, *161*, 35.
(25) Johnson, S.; Markwitz, A.; Rudolphi, M.; Baumann, H.; Oei, S. P.; Teo, K. B. K.; Milne, W. I. *Appl. Phys. Lett.* **2004**, *85*, 3277.
(26) Yu, J.; Qi, L. *J. Hazard. Mater.* **2009**, *169*, 221.
(27) Breedon, M.; Spizzirri, P.; Taylor, M.; Du Plessis, J.; McCulloch, D.; Zhu, J.; Yu, L.; Hu, Z.; Rix, C.; Wlodarski, W.; Kalantar-Zadeh, K. *Cryst. Growth Design* **2010**, *10*, 430.
(28) Lassner, E.; Schubert, W.-D.; *Tungsten: Properties, Chemistry, Technology of the Element, Alloys, and Chemical Compounds*; Kluwer Academic: New York, 1999.
(29) Bruyère, S.; Potin, V.; Gillet, M.; Domenichini, B.; Bourgeois, S. *Thin Solid Films* **2009**, *517*, 6565.
(30) Hassani, H.; Marzbanrad, E.; Zamani, C.; Raissi, B. *J. Mater. Sci: Mater. Electron* **2011**, in press; DOI: 10.1007/s10854-011-0297-x.
(31) Song, X C.; Zheng, Y. F.; Yang, E.; Wang, Y. *Mater. Lett.* **2007**, *61*, 3904.
(32) Gu, Z.; Zhai, T.; Gao, B.; Sheng, X.; Wang, Y.; Fu, H.; Ma, Y.; Yao, J. *J. Phys. Chem. B* **2006**, *110*, 23829.
(33) Modinos, A. *Field, Thermionic, and Secondary Electron Emission Spectroscopy*; Plenum Press: New York, 1984.
(34) Read, F. H.; Bowring, N. J. *Nucl. Instrum. Methods Phys. Res.* **2004**, *A 519*, 305.